International Journal of Chemical Studies

P-ISSN: 2349–8528
E-ISSN: 2321–4902
IJCS 2019; 7(5): 1261-1272

Received: 06-07-2019
Accepted: 24-07-2019

UK Maurya
National Institute of Abiotic Stress Management (NIASM), Malegaon, Baramati, Pune, Maharashtra, India

RA Duraiswami
Department of Geology, University of Pune, Pune, Maharashtra, India

NR Karmalkar
Department of Geology, University of Pune, Pune, Maharashtra, India

KPR Vittal
National Institute of Abiotic Stress Management (NIASM), Malegaon, Baramati, Pune, Maharashtra, India

Correspondence
UK Maurya
National Institute of Abiotic Stress Management (NIASM), Malegaon, Baramati, Pune, Maharashtra, India

Present Address:
Division of Soil Science & Agronomy, ICAR-Indian Institute of Soil & Water Conservation, Dehradun, Uttarakhand, India

Geochemical variability of major and trace elements and their role in abiotic stresses

UK Maurya, RA Duraiswami, NR Karmalkar and KPR Vittal

DOI: https://doi.org/10.22271/chemi.2019.v7.i5w.7116

Abstract
Geochemical variability in rocks collected from profile section, drilling core and random samples from NIASM site has been studied using x-ray fluorescence spectrometry. The sum total of all the major oxide analyses show variable degrees of weathering and range from highly weathered samples to fresh rock. Analyses were used on an anhydrous basis in the SINCLAS programme to recalculate major oxides and normalise the geochemical analyses to 100. The programme also gives a rock name following the TAS diagram as well as fixes the Fe_2O_3: FeO ratio and then calculates the norm. Based on the normative mineralogy and SiO_2 vs. Na_2O+K_2O content in the TAS diagram the present samples were classified into sub-alkaline basalts, basaltic andesites and andesite. Major oxide variation diagram in the Main Pit indicated silica and alumina oxides tend to accumulate towards the upper parts whereas TiO_2 and FeO tend to be mobile in an oxidizing environment and get leached towards the lower parts of the weathering profile. The unique lobate geometry of the lava flow does not weather uniformly resulting in a rather jagged oxide variation diagram which is predominantly a function of the lobe geometry and the porosity and permeability of the lobe sub-units. The Mg# of the subalkaline basalt indicates moderately evolved magmas. The trace element Cu and Ni have a distinctly opposite signature as compared to Zr, V, Cr, Zn, and Co. Concentration of Ba, Sr and Rb are invariably high in the upper and lower parts of the Main Pit which is due to modal variations in the plagioclase content or due to the variable mobility of these elements in response to differential weathering across the Main Pit profile. Anomalous concentration of different major oxides and trace elements at 50 cm and 70 cm depth is due to presence of the thin clay horizons related to weathering of glassy rind of a single 20 cm thick pahoehoe toe. Such anomalous accumulations could suggest that the clays provide suitable sites for their adsorption or that considerable enrichment of these elements takes place due to deposition of soluble salts in an oxidizing environment.

Keywords: Geochemical variability, abiotic stresses, basalt, pahoehoe toe

1. Introduction
The National Institute of Abiotic Stress Management (NIASM) site is a part of the Nira River Basin of the Upper Bhima River. Earlier work in the basin has been carried out by Kale *et al* (1993) [12], Rajguru *et al*. (1993) [24], Kale and Dasgupta (2009) [11], and Ghodke *et al*. (1984) [9]. Geological Survey of India (GSI, 1998) [8] has undertaken detailed mapping of the area and has classified the flows into the Dive Ghat Formation. The detailed chemostratigraphy of the area was undertaken by Khadri *et al*. (1999) [15] and the flows exposed in the basin have been classified as those belonging to the Poladpur and Ambenali Formation of Wai Subgroup. Duraiswami *et al* (2008a) [5] also reported rubbly pahoehoe flows from the Dive Ghat section. It has been observed that the multi-lobed compound geometry of the pahoehoe lava flow exposed at site has considerable control on weathering and mobility of major and trace element. The objectives of the present investigations are to study the geochemical variability in major and trace elements in the main pit at the site due to diverse nature of lobate geometry with different degree of weathering from inner to outer side of the lobes and establish the relationship with similar rocks exposed elsewhere in the site.

2. The study area
The NIASM site under study is located between N 18º8’59.279" and 18º9'45.845" and E 74º29'30.38" and 74º30'38.299" and lies between Karha Basin of Bhima River in the north and Nira River Basin in the south. It lies in the Drought Prone Area of plateau region of western Maharashtra on a water divide with a smooth but slightly undulating topography within the limits of village Malegaon Khurd, Baramati Taluka of Pune district. The area is known for its frequent scarcity. The site is well connected by road with major cities in the State and also by

Central Rail Network to Pune via Daund Junction (Fig.1).

Fig 1: Location of study area Malegaon in Pune District

The side of the area is drained by two streams and generally exhibit dendritic drainage pattern especially in the lower order streams. A prominent percolation tank is built across the western stream while an earthen dam is built across the eastern stream. The climate of the region is semi-arid dry. Based on the rational classification of climate (Potential evapo-transpiration and Moisture index), the study area experiences arid megathermal climate (Paranjape, 2001) [22].

3. Material and Methods

Rock samples from surfacial pits and boreholes were selected for geochemical analyses and were optimized on the basis of the representations in the basaltic weathering profile at NIASM project site. Eight representative samples each from the main pit and the boreholes and ten representative samples from random surfacial locations from NIASM site were selected for major oxide and trace element analyses. Small chips of each sample (~150 gm) were broken by a steel hammer, rinsed several times with ultra-pure water and crushed with an agate mortar and pestle and pelletized into pellets using 4 grams of sample powder mixed with 0.7 grams of wax at 10 tons/in^2 pressure using a hydraulic press. Samples for both major and trace elements were analyzed after calibrating internal standards using SPECTRO ED-XRF. The standard deviation for all major oxides is less than 0.5, except for SiO_2 and Na_2O where it is around 1. The LIO was not determined for these samples and the analyses were used on an anhydrous basis in the SINCLAS programme (Verma *et al*., 2002) [26] to recalculate major oxides and normalize the geochemical analyses to 100. Total iron was split into ferrous and ferric oxides on the basis of well-established criteria. In the measured iron-oxidation ratio option, all iron was considered as Fe_2O_3 ($_T$) the Middlemost option (Middlemost, 1989) [21] was used, which proposed a fixed ratio of Fe_2O_3 to FeO that depended on the rock type (Classification).

4. Results and Discussion

4.1 Geological variability of the site

The rocks exposed in the study area belong to Cretaceous age. The Recent deposits are represented by shallow alluvium whereas the Quaternary is represented by consolidated sediments exposed in the downstream of the study areas. Two lava flows of varying thickness and morphology belonging to the Deccan Traps are exposed in the study area. The lowermost flow F1 is grey, fine-grained, jointed and simple. It is exposed only in the well sections in the study area as well at places where upper flow has been removed by denudation and weathering action. The upper flow F2 is pinkish, vesicular and belongs to the hummocky pahoehoe type. The flow is strongly compound and consists of lava toes, meter scale lobes and thick (~10m) sheet lobes. The vesicles in this flow are small (1-2 cm) and invariably filled with zeolites and other secondary minerals like calcite. The base of individual lava units are marked by pipe-amygdales. The upper flow F2 is extensively exposed in the NIASM site and in the adjacent well sections. An elaborate geochemical (Beane *et al*., 1986) [2] and lithostratigraphy (GSI, 1986, Godbole *et al*. 1996) [10] exists for the Western Deccan Traps (Table 1). Detailed mapping in the adjacent areas has revealed the lower simple flow belongs to the Indrayani Formation (Godbole *et al*. 1996) [10] equivalent to the Khandala Formations (Khadri *et al*. 1999) [15] while the upper compound hummocky pahoehoe flow belongs to the Karla Formation (GSI, 1986, Godbole *et al*. 1996) [10] or Bushe Formations (Duraiswami, 2009) [4].

Table 1: Established geochemical and lithostratigraphy in the western Deccan Traps (After Beane *et al*., 1986, GSI 1986, Godbole *et al*. 1996) [2, 10].

Geochemical stratigraphy			*Lithostratigraphy*			
Group	**Sub-group**	**Formation**	**Super Group**	**Group**	**Sub Group**	**Formation**
DECCAN BASALT	Wai	Desur	DECCAN TRAP	SAHYADRI GROUP	Mahabaleshwar	Mahabaleshwar
		Panhala				**M4**
		Mahabaleshwar				
		Ambenali			Diveghat	Purandargad
		Poladpur				Diveghat
					Lonavala	Elephanta
	Lonavala	Bushe				Karla
		Kandhala				Indrayani
						M3
	Kalsubai	Bhimashankar			Kalsubai	Upper Ratangad
		Thakurwadi				**M2**
		Neral				Lower Ratangad
		Igatpuri				**M1**
		Jawhar				Salher

A rectangular pit (l:8m, b:2.5m, d:3m) was dug towards the south-central part of the NIASM site and is referred to as the main pit (MP) (Fig. 2). The pit exposes a weathering profile typical of compound pahoehoe flows (Bondre *et al*., 2004) [3].

Fig 2: Main Pit

An intricate geometry of lava lobes and toes is seen on the eastern face of the main pit (Fig. 3). Most of the lava toes and lobes are completely vesicular and can be classified as s-type lobes of Wilmoth and Walker (1993) [27] (Fig. 4a).

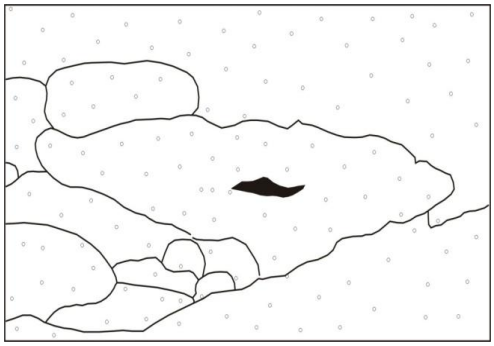

Fig 3: Field sketch of the lobate geometry of the compound pahoehoe flow exposed in the NIASM site.

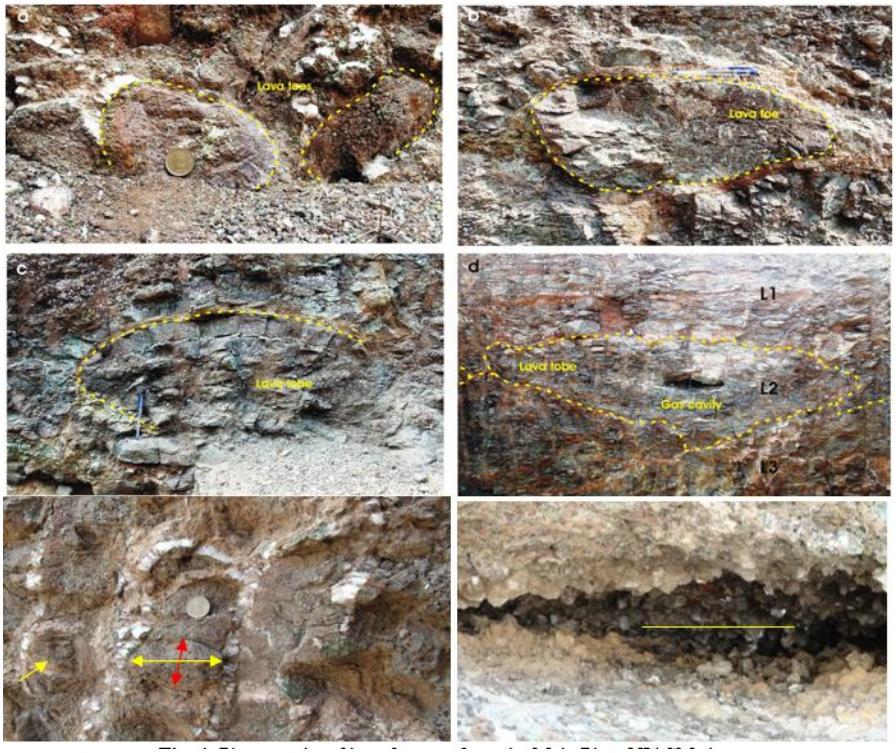

Fig 4: Photographs of lava features from the Main Pit at NIASM site.

The southern face of the MP exposes three distinct lava lobes. The upper lobe is partially exposed and has developed a crude weathering profile. The middle lobe is intact and is completely exposed in cross section in the MP (Fig. 4b). The lobe is augen shaped and has a length of 1m and thickness of 0.5m. It consists of the typical 3-tiered internal structure of crust-core-basal zone of Aubele *et al*., (1988) [1] but is characterized by the lack of pipe vesicles in the basal vesicular zones and thus, this relatively large lava lobe also belongs to the s-type lobes. The crust of this lobe is highly vesicular and at places develops a crude vesicle banding. The vesicles are small towards the chilled margins of the lobes but become larger (up to 2 cm) towards the base of the crust. The western face of the MP exposes a chaotic assemblage of small lava toes (Fig. 4c) and lobes as well as large dome shaped lobe (Fig. 4d). The inter-lobe spaces are highly weathered and show beautiful zeolite mineralization (Fig. 4E). A large 40 cm central gas blister or cavity is seen towards the mid central part of the lobe and is lined by zeolites (Fig. 4F). The detailed lithologs of samples collected from the MP is presented in Table 2.

Table 2: Geological logs from main pit at NIASM site

Sr. no.	Depth (cm) From	To	Sample No	Description
1	0	17	MP1	Highly weathered basalts with few zeolite filled vesicles
2	17	27	MP2	Weathered basalt with fluffy white zeolite encrustation with few zeolite filled vesicles.
3	27	50	MP3	Fine grained, reddish bole (Glassy rind of weathered pahoehoe lobe) with small white patches of calcrete
4	50	65	MP4	Light brown, moderately weathered basalt with 0.2 to 0.9 mm spherical vesicles partly filled with buff coloured zeolite and also one side with white patches of calcrete/zeolite (?)
5	65	70	MP5	Sample similar to MP3, probably lower rind of pahoehoe lobe, no calcrete deposition seen here unlike MP3 and sample slightly harder than MP3.
6	70	83	MP6	Grayish brown moderately weathered basalt with 0.22 to 0.5 mm white amygdales filled with zeolites.
7	83	156	MP7	Grayish moderately weathered basalt with < 2 mm spherical vesicles which contains greenish lining and zeolite mineralization.
8	156	231	MP8	Sample similar to MP7 except the presence of one 3 mm white amygdale and more weathered than MP7

Besides this core drilling was conducted to 5m depths at numerous locations from NIASM for geotechnical investigations. The cores were inspected and logged and chips were harvested for detailed geochemical investigations. Random samples were also collected from areas and are represented on the NIASM site (Fig. 5) so that weathering patterns and inter borehole correlations could be established. The detail lithologs of sample collected from cores and random sampling are shown in Table 3 & 4.

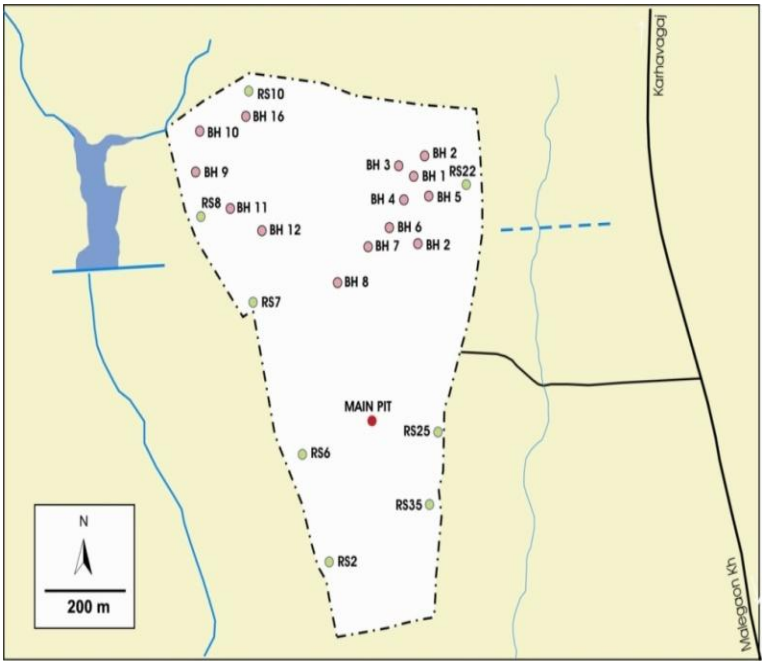

Fig 5: Sample location at NIASM Site. Main Pit (MP), Bore Hole Pit (BH 1-12 &16) and Random Sample Pit (RS 2, 6, 7,8,10, 12, 25 &35)

Table 3: Geological logs from the different boreholes at NIASM site

Sr. no.	Depth (m) From	To	Sample No	Description
1	4.5	5.0	BH-1/28	Fresh, brownish, massive basalt with dixytaxitic texture, without vesicles.
2	1.5	2.5	BH-9/1	Reddish brown, vesicular basalt with fine zeolites lining the vesicles.
3	4.0	4.5	BH-9/18	Reddish brown massive basalt devoid of vesicles.
4	4.5	5.0	BH-9/22	Reddish brown massive basalt with minute < 1 mm vesicles and some of them are filled with zeolites.
5	3.5	5.0	BH-10/19	Grayish black massive basalt with large stray vesicles filled by zeolites.
6	0.2	1.0	BH-7/3	Brownish massive basalt.
7	4.0	5.0	BH 7/31	Red coloured, highly zeolitised massive basalt.

Table 4: Geological logs from various random locations at the NIASM site

Sr. no.	Depth (m) From	To	Sample No	Description
1	0.2	1.2	RS2	Reddish vesicular basalt, moderately weathered, few large (~10cm) elongated vesicles, partly filled with zeolites.
2	0.3	1.5	RS6	Reddish brown comparatively fresh basalt with numerous partly filled vesicles.
3	1.0	1.5	RS7	Comparatively fresh reddish grey, fine grained basalt representing massive part of the lava lobe with fine dixytaxitic texture.
4	0.8	1.4	RS8	Comparatively fresh reddish basalt with 0.2 mm to 0.5 mm vesicles lined creamish material, non zeolite bearing.
5	0.3	0.9	RS10	Moderately weathered fine grained basalt showing plain surfaces (joints) along which greenish encrustations of fine zeolite are deposited.
6	0.1	1.3	RS11	Comparatively fresh dense basalt with high vesicle density of spherical to irregular filled with zeolites
7	0.3	1.1	RS17	Comparatively fresh, grey, massive basalt devoid of zeolites but with minute irregular pores (dixytaxitic texture).
8	0.2	1.0	RS25	Sample similar to RS17, but comparatively more weathered.
9	0.1	1.3	RS26	Massive, dense, comparatively weathered basalt where dixytaxitic voids are filled with zeolites.
10	0.3	1.6	RS36	Reddish brown, moderately weathered basalt with small (~2 mm) vesicles filled by platy zeolites.

4.2 Geochemical variability in major oxide

The analytical results of major oxide and their normative classification are given in the table 5 to 7. Based on normative classification most of the samples analysed belongs to sub-alkaline, tholeiite (hypersthene normative) basalts. Besides this, most fresh samples are olivine normative with the normative olivine content varying from 3.28 to 6.48. This geochemical observation.

Table 5: Major oxide geochemistry and CIPW norms of samples from main pit of NIASM site

Sample	MP 1	MP 2	MP 3	MP 4	MP 5	MP 6	MP 7	MP 8
Rock type	B, subal	B, subal	B, subal	B, subal	A	B, subal	BA	B, subal
SiO_2	44.25	43.44	35.94	44.48	42.34	44.81	43.26	45.13
TiO_2	2.21	1.92	0.46	2.28	0.58	2.04	1.90	2.55
Al_2O_3	8.94	9.56	11.11	8.47	12.58	9.64	9.32	7.95
$Fe_2O_3(T)$	12.06	11.89	3.85	13.88	5.14	12.54	11.28	15.00
MnO	0.17	0.13	0.04	0.17	0.05	0.16	0.12	0.15
MgO	4.59	3.69	1.66	3.65	3.49	4.95	5.21	6.12
CaO	12.95	10.46	19.92	10.32	8.19	10.75	7.99	7.07
Na_2O	1.67	2.76	0.17	3.14	1.28	2.34	2.96	3.50
K_2O	0.37	0.58	0.05	0.27	0.31	0.37	0.46	0.45
P_2O_5	0.16	0.25	0.03	0.28	0.03	0.20	0.20	0.29
Total	87.37	84.68	73.23	86.94	73.99	87.80	82.70	88.21
SiO_2adj	51.25	51.92	49.30	51.87	57.53	51.66	52.88	51.91
TiO_2adj	2.56	2.30	0.63	2.66	0.79	2.35	2.32	2.93
Al_2O_3adj	10.35	11.43	15.24	9.88	17.09	11.11	11.39	9.15
Fe_2O_3adj	2.13	2.17	0.81	2.47	1.67	2.21	2.93	2.63
FeOadj	10.65	10.84	4.03	12.34	4.78	11.03	9.77	13.16
MnOadj	0.20	0.16	0.06	0.20	0.07	0.18	0.15	0.17
MgOadj	5.32	4.41	2.28	4.26	4.74	5.71	6.37	7.04
CaOadj	15.00	12.50	27.32	12.03	11.13	12.39	9.77	8.13
Na_2Oadj	1.93	3.30	0.23	3.66	1.74	2.70	3.62	4.03
K_2Oadj	0.43	0.69	0.07	0.32	0.42	0.43	0.56	0.52
P_2O_5adj	0.19	0.30	0.04	0.33	0.04	0.23	0.24	0.33
Q	4.33	0.79	3.72	0.96	15.92	2.44	1.78	-
Or	2.53	4.10	0.40	1.86	2.49	2.52	3.32	3.06
Ab	16.37	27.92	1.97	30.98	14.72	22.83	30.62	34.07
An	18.31	14.32	40.33	9.58	37.59	16.96	13.18	5.35
Di	45.49	38.21	51.11	40.31	14.07	35.66	27.60	27.14
Hy	4.60	6.47	-	6.93	11.21	11.41	14.27	16.50
Ol	-	-	-	-	-	-	-	3.73
Mt	3.09	3.14	1.17	3.58	2.43	3.20	4.25	3.81
Il	4.86	4.36	1.20	5.05	1.50	4.47	4.41	5.57
Ap	0.43	0.69	0.10	0.76	0.10	0.53	0.57	0.77
Mg#	47.08	42.04	50.20	38.07	63.88	47.99	53.75	48.82
$FeO(T)$//MgO	2.36	2.90	2.09	3.42	1.33	2.28	1.95	2.21
Salic	41.53	47.12	46.43	43.38	70.71	44.74	48.90	42.48
Femic	36.28	31.67	14.60	32.60	24.77	37.71	39.59	44.13
CI	71.05	54.45	66.72	48.24	63.53	61.08	54.82	44.26
DI	23.22	32.80	6.10	33.80	33.12	27.79	35.71	37.13
SI	25.98	20.60	30.73	18.47	35.51	25.87	27.39	25.72
AI	1.21	1.40	1.01	1.44	1.17	1.31	1.49	1.71

WI	3610	3945	3167	3890	2537	3719	3780	4050

B, subal-Basalt, subalkaline; BA-Basaltic andesite; A-Andesite. CI-Colour Index, AI-Alkalinity Index, WI-Weathering Index, SI-Silica Index

Table 6: Major oxide geochemistry and CIPW norms of samples from the boreholes at the NIASM site

Sample	**BH1/80**	**BH7/3**	**BH7/13**	**BH9/1**	**BH9/2**	**BH9/18**	**BH10/9**	**BH10/19**
Rock type	**B, subal**	**B, subal**	**BA**	**BA**	**BA**	**B, subal**	**B, subal**	**B, subal**
SiO_2	47.23	46.90	48.38	47.50	46.72	45.67	45.79	46.85
TiO_2	2.61	2.65	2.04	2.12	1.96	2.39	2.23	2.32
Al_2O_3	12.20	12.19	10.65	10.74	10.10	11.85	12.43	12.50
Fe_2O_3 (T)	12.74	12.64	12.54	12.20	11.78	13.60	13.11	13.13
MnO	0.16	0.20	0.18	0.17	0.17	0.30	0.20	0.20
MgO	5.52	5.05	4.58	4.04	4.77	5.62	5.65	4.79
CaO	12.12	13.00	11.21	9.99	9.02	12.89	11.85	11.11
Na_2O	2.89	2.78	2.52	2.41	3.04	2.50	2.54	2.76
K_2O	0.40	0.22	0.48	0.48	0.66	0.15	0.22	0.29
P_2O_5	0.22	0.24	0.21	0.19	0.19	0.19	0.21	0.21
Total	92.54	88.13	86.24	93.79	99.92	91.99	94.23	94.16
SiO_2adj	49.71	49.47	52.70	53.44	53.41	48.58	49.18	50.35
TiO_2adj	2.75	2.80	2.22	2.39	2.24	2.54	2.40	2.49
Al_2O_3adj	12.84	12.86	11.60	12.08	11.55	12.61	13.35	13.43
Fe_2O_3adj	2.05	2.03	2.90	2.92	2.86	2.21	2.15	2.15
FeOadj	10.23	10.17	9.68	9.73	9.54	11.03	10.74	10.76
MnOadj	0.17	0.21	0.20	0.19	0.19	0.32	0.22	0.22
MgOadj	5.81	5.33	4.99	4.55	5.45	5.98	6.07	5.15
CaOadj	12.76	13.71	12.21	11.24	10.31	13.71	12.73	11.94
Na_2Oadj	3.04	2.93	2.75	2.71	3.48	2.66	2.73	2.97
K_2Oadj	0.42	0.23	0.52	0.54	0.75	0.16	0.24	0.31
P_2O_5adj	0.23	0.25	0.23	0.21	0.22	0.20	0.23	0.23
Q	-	-	5.20	7.53	3.10	-	-	0.42
Or	2.49	1.37	3.09	3.19	4.46	0.95	1.40	1.84
Ab	25.74	24.81	23.23	22.95	29.41	22.50	23.08	25.10
An	20.14	21.24	17.79	19.20	13.68	21.99	23.48	22.42
Di	34.31	37.30	34.13	29.14	29.70	36.99	31.53	29.34
Hy	3.61	3.24	7.60	8.73	10.76	2.60	7.93	12.50
Ol	4.99	3.20	-	-	-	6.48	4.40	-
Mt	2.97	2.95	4.21	4.23	4.15	3.20	3.11	3.12
Il	5.22	5.31	4.22	4.53	4.25	4.83	4.55	4.74
Ap	0.54	0.59	0.53	0.50	0.50	0.47	0.52	0.52
Mg#	50.32	48.29	47.88	45.45	50.47	49.13	50.19	46.03
FeO(T)/MgO	2.08	2.25	2.46	2.72	2.22	2.18	2.09	2.47
Salic	48.37	47.42	49.30	52.88	50.64	45.43	47.96	49.78
Femic	36.12	34.98	34.52	32.72	36.05	36.91	37.22	35.25
CI	65.70	67.71	60.36	55.04	54.14	68.70	65.65	58.70
DI	28.23	26.18	31.52	33.67	36.96	23.45	24.48	27.36
SI	26.97	25.74	23.94	22.24	24.69	27.13	27.69	24.13
AI	1.31	1.27	1.32	1.32	1.48	1.24	1.26	1.30
WI	4316	4183	3934	3637	4084	4014	3948	3929

Table 7: Major oxide geochemistry and CIPW norms of random samples from the NIASM site

Sample	**RS 2**	**RS 6**	**RS 7**	**RS 8**	**RS 10**	**RS 11**	**RS 17**	**RS 25**	**RS 26**	**RS 35**
Rock type	**B, subal**	**B, subal**	**B, subal**	**B, subal**	**BA**	**B, subal**	**B, subal**	**B, subal**	**B, subal**	**BA**
SiO_2	45.83	45.39	42.02	45.38	48.33	42.42	45.54	49.13	45.26	48.56
TiO_2	2.40	2.22	2.15	2.22	1.92	2.22	2.21	2.75	2.28	1.88
Al_2O_3	11.97	11.81	11.23	11.51	10.60	11.69	11.54	13.27	10.64	10.55
Fe_2O_3(T)	13.39	12.20	12.47	13.03	10.71	12.33	13.20	13.32	12.68	11.32
MnO	0.17	0.15	0.15	0.17	0.17	0.17	0.20	0.20	0.17	0.13
MgO	5.07	3.91	5.72	5.73	3.77	4.07	7.02	5.27	4.99	5.17
CaO	11.85	11.37	11.40	11.83	8.77	11.20	11.40	12.41	9.54	9.34
Na_2O	2.41	1.88	1.77	2.24	2.05	1.69	2.13	3.11	2.50	2.20
K_2O	0.19	0.20	0.21	0.22	0.64	0.26	0.32	0.17	0.71	0.51
P_2O_5	0.22	0.17	0.20	0.21	0.17	0.19	0.23	0.29	0.22	0.18
Total	93.50	89.30	87.32	92.54	85.13	86.24	93.79	99.92	88.99	86.84
SiO_2adj	49.62	51.43	48.71	49.63	56.01	49.79	49.14	49.73	51.48	54.59
TiO_2adj	2.60	2.52	2.49	2.43	2.23	2.61	2.39	2.78	2.59	2.11
Al_2O_3adj	12.96	13.38	13.02	12.59	12.29	13.72	12.45	13.43	12.10	11.86
Fe_2O_3adj	2.21	2.11	2.21	2.17	2.64	2.21	2.17	2.06	2.20	2.71
FeOadj	11.06	10.54	11.02	10.87	8.80	11.04	10.86	10.28	11.00	9.02
MnOadj	0.18	0.17	0.17	0.19	0.20	0.20	0.22	0.20	0.19	0.15

MgOadj	5.49	4.43	6.63	6.27	4.37	4.78	7.58	5.34	5.68	5.81
CaOadj	12.83	12.88	13.22	12.94	10.16	13.15	12.30	12.56	10.85	10.50
Na_2Oadj	2.61	2.13	2.05	2.45	2.38	1.98	2.30	3.15	2.84	2.47
K_2Oadj	0.21	0.23	0.24	0.24	0.74	0.31	0.35	0.17	0.81	0.57
P_2O_5adj	0.24	0.19	0.23	0.23	0.20	0.22	0.25	0.29	0.25	0.20
Q	0.47	6.09	-	0.09	12.91	3.62	-	-	1.67	9.10
Or	1.22	1.34	1.44	1.42	4.39	1.80	2.04	1.02	4.78	3.39
Ab	22.08	18.02	17.36	20.73	20.11	16.79	19.45	26.64	24.07	20.93
An	23.04	26.28	25.59	22.64	20.66	27.63	22.65	22.01	17.87	19.57
Di	32.38	30.32	31.69	33.05	23.54	30.10	30.16	31.73	28.43	25.59
Hy	12.12	9.68	15.28	13.77	9.89	11.40	14.14	7.17	14.50	13.01
Ol	-	-	0.17	-	-	-	3.32	2.49	-	-
Mt	3.21	3.06	3.20	3.15	3.82	3.20	3.15	2.98	3.19	3.92
Il	4.94	4.78	4.73	4.61	4.23	4.95	4.53	5.29	4.93	4.02
Ap	0.55	0.45	0.54	0.53	0.46	0.52	0.57	0.68	0.58	0.47
Mg#	46.95	42.83	51.74	50.69	46.96	43.55	55.42	48.05	47.91	53.47
$FeO(T)/MgO$	2.38	2.81	1.96	2.05	2.56	2.73	1.69	2.27	2.29	1.97
Salic	46.81	51.73	44.39	44.88	58.06	49.84	44.13	49.67	48.38	52.99
Femic	37.08	32.03	41.26	39.80	30.64	34.14	43.14	35.07	37.65	36.29
CI	63.42	60.61	69.93	67.04	51.55	62.70	68.86	62.75	55.32	57.82
DI	23.76	25.45	18.80	22.24	37.40	22.21	21.48	27.65	30.51	33.42
SI	25.45	22.80	29.93	28.49	23.09	23.52	32.58	25.41	25.20	28.24
AI	1.25	1.20	1.19	1.24	1.32	1.19	1.24	1.29	1.38	1.32
WI	3785	3293	3444	3783	3355	3226	3882	4272	3914	3574

Corroborates with the fact that the petrography of unaltered basalts contain modal olivine. Other samples analysed contain variable amount of normative quarts (0.42 to 12.91) which is recorded in moderately to highly weathered samples. The proportion of normative quartz increases with increase in the degree of weathering. Based on the normative mineralogy and plotting silica (SiO_2) vs. total alkalis (Na_2O+K_2O) content in the TAS diagram the present samples were classified into sub-alkaline basalts (B, subal), basaltic andesites (BA) and andesite (A) (Fig. 6). The basalts showing up as basaltic andesites and andesite are invariably vesicular basalts with variable zeolite mineralization or highly weathered vesicular basalts where highly mobile oxides have been leached relative to silica.

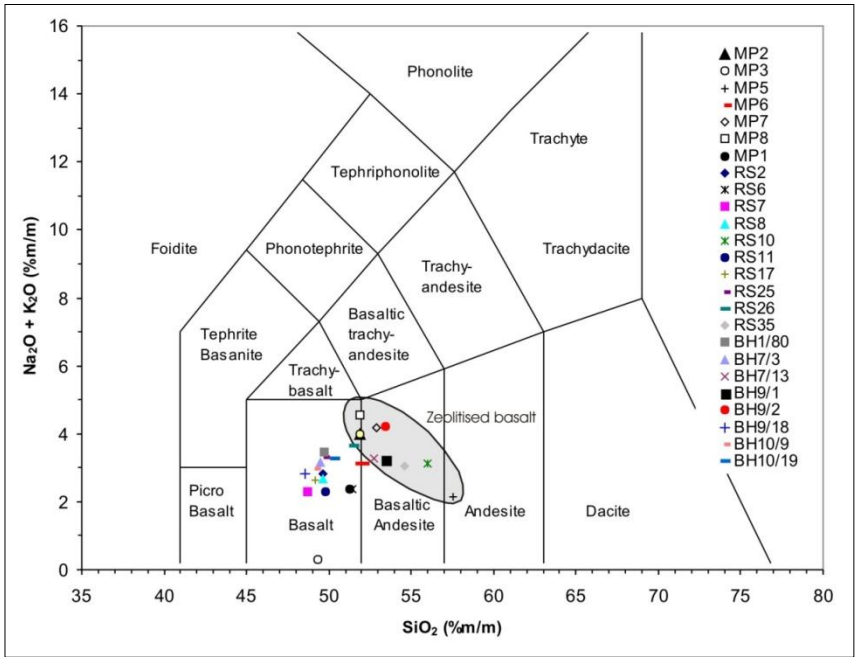

Fig 6: Total Alkali-Silica (TAS) diagram for basalt samples from the NIASM

Although a total of 26 samples were analysed in the present study, the samples from the Main Pit (MP) were used to depict the geochemical variation across a weathering profile of compound pahoehoe as the lobate geometry of the pahoehoe units were better understood in the Main Pit. Major oxide variation diagram (Fig. 7) of samples from main pit indicated silica (SiO_2) content varies from 49.30 wt.% to as high as 57.53 wt.% in the present study. The TiO_2 content varies from 0.63 to 2.93 wt.% and as such belong to the low Ti-basalts of the Deccan Traps. Alumina (Al_2O_3) content varies from 9.88 to 17.09 wt % with a exceptionally high content of 17.09 wt.% for sample MP5. MgO content in the samples varies from 2.28 to 7.04 wt.% while CaO from 8.13 to15.0 wt.% (Table 5). High CaO could be related either to high modal plagioclase content in the basalt or the presence of secondary mineralization of calcite or common alteration product calcrete. The alkalis (Na_2O, K_2O) show variable content depending on the affects of alteration and degree of weathering the individual samples had undergone. The Na_2O content varies from 1.74 to 4.03 wt.% while K_2O varies from

0.04 to 0.33 wt.%. The Mg# of the subalkaline basalt varies from 38.07 to 55.42 and indicates moderately evolved magmas. Higher Mg# (53.75 to 63.88) is recorded in the basaltic andesites and andesite sample which reflect a pseudo increase due to secondary mineralization or relative enrichment in the samples analysed (Table 5 & Fig. 7). The normative mineralogy was used to calculate Colour Index (CI) of the samples that varies from 54.14 to 71.05 and the Alkalinity Index (AI) from 1.01 to 1.71.

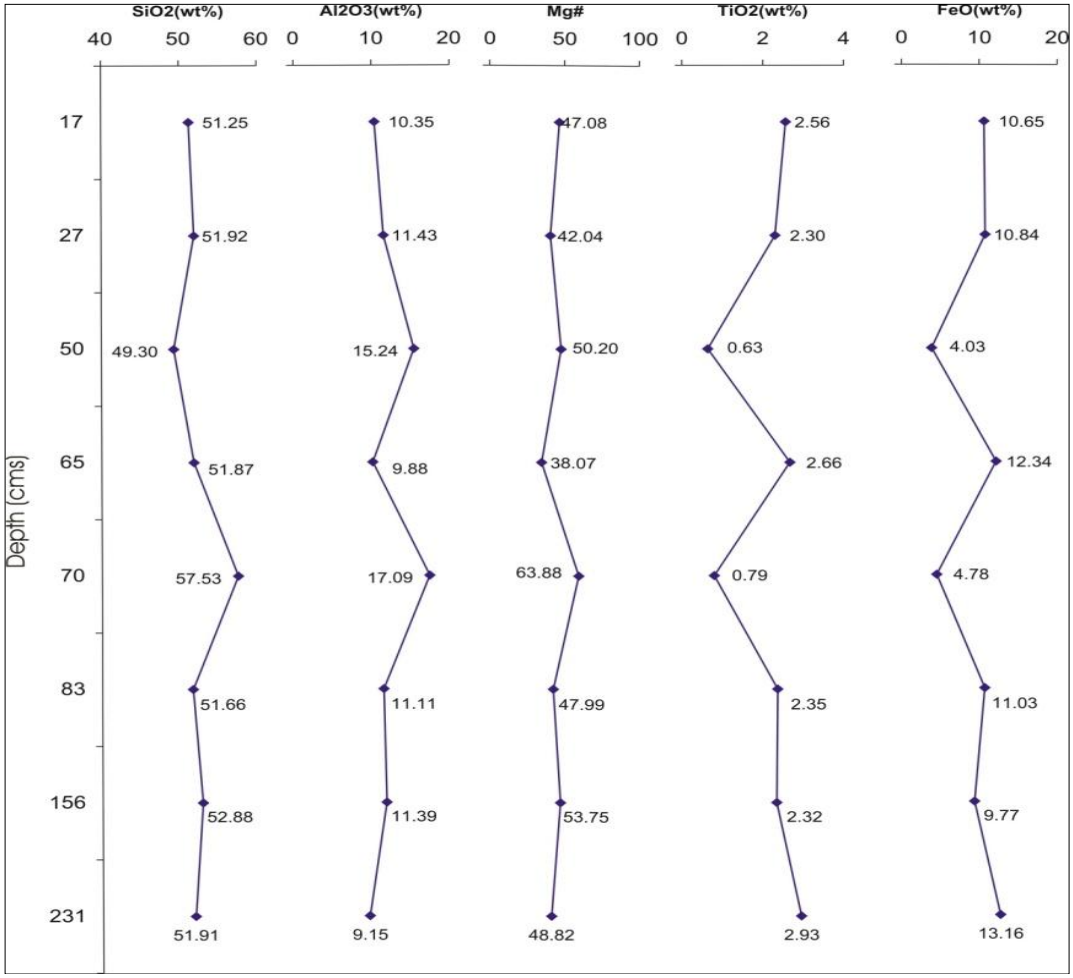

Fig 7: Major oxide variation diagram with depth in main pit samples from the NIASM site. #Mg in countsn

Figure 7 indicates an anomalous concentration of different major oxides at 50 cm and 70 cm depth due to presence of the thin clay horizons related to weathering of glassy rind of a single 20 cm thick pahoehoe toe. There is a perceptible increase in the alumina and magnesia contents at the upper interface of the toe (at 50 cm) while there is a perceptible decline in the TiO_2 and FeO at the same interface. Similar oxide pattern is also pronounced at the lower interface at 70 cm. From the major oxide variation diagram it is clear that oxides such as silica and alumina which are relatively immobile during weathering and leaching tend to accumulate towards the upper parts of the weathering horizons. In contrast the oxide such as TiO_2 and FeO tend to be mobile in an oxidizing environment and get leached towards the lower parts of the weathering profile. The unique lobate geometry of the lava flow however does not weather uniformly as individual lobes and their sub-units tend to weather independently, especially in the initial stages of weathering. This result in a rather jagged oxide variation diagram which is predominantly a function of the lobe geometry and the porosity and permeability of the lobe sub-units. This is reflected in the Main Pit at the NIASM site where three distinct lobes are exposed. The oxide variations can be better explained by taking the examples of the relatively mobile elements like titania and iron. The upper lobe is partially exposed at the Main Pit of the NIASM site and is exposed to the hydrometerological elements that break down mineral constituents like plagioclase, augite, olivine and glass to release iron and titania. Being mobile these tend to get leached and move downwards. At 50 cm of the profile, the glassy upper rind tends to be unstable in the weathering regime and has weathered to a great extent there by rendering a rapid decline in the oxide values (Fig. 7). Similar type of situation exists at the 70 cm mark where the lower glassy rind occurs. The intermittent sample at 65 cm represents the vesicular core of the lava toe that has nearly the original oxide content due to relatively less weathering thereby giving a pseudo positive anomaly in the profile. Lobe 3 in the Main Pit occurs below 70 cm and is exposed incompletely until 2.30 m BGL. In this lobe a reversal of the weathering pattern is seen where in the degree of weathering is highest at 70 cm (at the red bole glassy horizon) up to 2.31 m where the original unweathered basalt is exposed. The steady increase in the oxide percentage from the weathered glassy rind to the host rock is also reflected in the major oxide pattern of this lobe. Also one can notice the difference in the nature of weathering in the upper and lower lobe. Hence, in weathering regimes of the compound pahoehoe the lobe geometry will dictate the weathering pattern which is in stark contrast to the weathering

pattern seen in the simple flows or conventional soil profiles in basalts.

4.3 Geochemical variability in trace element content and their role in the abiotic stresses

The analytical results of trace element analyses are presented in Tables 8 to 10 and variation diagram representative to main pit are shown in Fig. 8. There is a general variability in the trace element content of the samples analysed and this is a reflection of host basalt geochemistry and its weathering products. The biogeochemistry of the significant trace elements is discussed here so as to give a brief account of its role in the abiotic stress at NIASM site, Malegaon.

Table 8: Trace element concentrations (ppm) of samples from main pit of NIASM site

Sample	MP1	MP2	MP3	MP4	MP5	MP6	MP7	MP8
Rock type	B, subal	B, subal	B, subal	B, subal	A	B, subal	BA	B, subal
V	319	279	122	353	100	298	322	343
Cr	247	194	15.8	233	16.8	241	228	288
Co	47.2	30.4	19.6	41.2	23.3	29.7	30.7	58.1
Ni	114	96.9	144	105	227	105	97.1	125
Cu	172	145	441	247	577	128	145	142
Zn	90.4	90.5	47.3	92.7	63.1	97.4	76.5	104.5
Ga	19	10.1	43.5	9.1	30.6	16.6	16.5	20.6
Rb	15.9	13.1	4	6.2	23.1	17.5	22.3	24.9
Sr	374	541	77.9	280	1456	705	400	218
Y	25.2	25.3	6.6	34.3	4.4	26.5	30.5	39.9
Zr	119	123	58.9	142	72.4	127	121	160
Nb	8.0	7.0	8.5	8.8	5.6	5.8	5.5	10.4
Mo	6.2	4.3	2.6	5.5	1	4.0	4.0	6.0
Sn	14.2	16.7	13.1	15.9	12.7	12.5	14.8	12.6
Ba	241	420	51.0	118	360	134.2	191	103
Pb	3.4	1.9	4.1	1.0	5.2	2.7	2.5	5.0

Table 9: Trace element concentrations (ppm) of samples from the boreholes at the NIASM site

Sample	BH1/80	BH7/3	BH7/13	BH9/1	BH9/2	BH9/18	BH10/9	BH10/19
Rock type	B, subal	B, subal	BA	BA	BA	B, subal	B, subal	B, subal
V	464	416	317	312	315	378	363	386
Cr	203	213	256	179	187	221	234	185
Co	35.6	41.2	36.9	42.8	26.3	41.0	34.1	32.6
Ni	96.7	103.7	114.9	86.0	86.7	113.9	113.9	88.0
Cu	182	198	201	158	171	184	119	190
Zn	98.3	99.2	91.8	98.4	92.0	102.1	100.2	98.5
Ga	17.6	27.8	14.3	18.5	21.9	18.5	18.8	17.2
Rb	9.6	3.3	16.3	14.7	27.4	5.1	9.5	11.1
Sr	230	228	350	561	306	204	218	276
Y	32.3	31.3	27.9	25.6	26.7	28.9	27.5	27.5
Zr	149	149	125	132	127	135	132	140
Nb	8.0	8.5	6.5	7.0	6.8	8.3	7.0	6.9
Mo	5.5	4.9	4.8	3.8	3.8	5.2	5.0	5.4
Sn	14.7	11.0	12.4	11.4	12.4	16.5	8.6	16.7
Ba	70.3	79.5	171	214	133	86.7	64.3	103
Pb	2.7	2.8	2.0	1.0	2.9	2.1	2.2	2.5

Table 10: Trace element concentrations (ppm) of random samples from the NIASM site

Sample	RS2	RS6	RS7	RS8	RS10	RS11	RS17	RS25	RS26	RS35
Rock type	B, subal	B, subal	B, subal	B, subal	BA	B, subal	B, subal	B, subal	B, subal	BA
V	364	329	342	344	275	352	370	467	335	274
Cr	196	203	214	264	163	181	307	216	218	223
Co	31.3	35.7	35.9	41.5	14.2	28.4	45	31.4	44.1	35.5
Ni	94.1	77.1	120	113	77.4	77.9	146	100	94.2	104
Cu	192	175	165	162	132	170	153	181	181	167
Zn	105	91.0	92.9	107	84.7	94.5	102	104	106	86.2
Ga	22.4	20.4	21.7	22.7	14.6	20.0	22.2	24.3	19	18.5
Rb	5.4	8.1	9.9	12.4	28.1	15.2	19.3	2.2	35	19
Sr	251	319	172	191	383	187	192	234	551	169
Y	28	24.3	26	27.2	20.9	27.2	25.4	31.8	27.5	20.7
Zr	138	135	129	134	118	132	127	157	128	114
Nb	8.2	6.6	7.2	7.1	8.2	6.2	6.8	10.9	6.6	7.0
Mo	7.0	7.1	6.7	6.3	5.5	5.2	8.5	5.6	7.4	6.9
Sn	14.1	17	15.9	17.3	11.5	19	15.6	18.2	10.2	16.8
Ba	73.7	76.7	35	57.8	153	36.5	42.1	85.1	152	95.5
Pb	1.0	2.1	2.8	2.4	2.5	2.6	2.2	1.6	1.9	2.2

Vanadium (V) content in the samples analysed varies from 100 to 464 ppm and as such is within the normal range in the weathering profiles of Deccan Traps. The vanadium bearing blue zeolite - cavensite and phillipsite are common to basalt cavities in and around Pune. Vanadium enters the food chain through soil, vegetation and herbivorous animals. The cycle of vanadium initiates with the weathering of the basalt under a relatively high redox potential. It is generally adsorbed on to clays and is released into the hydrosphere only by humic solutions. Highly alkaline surface waters and groundwater with calcite in the oxidizing weathering profile could precipitate small quantities of Pb, Cu, Zn or U vanadates. The presence of vanadium in the weathering mantle of the NIASM site indicates that the flora (crops, fodder) and fauna (poultry, cattle) to be raised on the experimental plots may not be stressed due to vanadium deficiency. Cobalt (Co) and nickel (Ni) are widely distributed in the biosphere and in the present study their concentrations varies from 14 to 58 ppm and 77 to 146 ppm respectively. In basalts, the Co and Ni behave similarly and generally reside in minerals such as olivine and augite which are main constituents of basalts. In the weathering profile, Co remains in solution as bicarbonate, in contrast, Ni tends to accumulate in the insoluble weathering residue. Deficiency of Cobalt in soils and subsequently in cattle fodder is the established cause of 'bush sicknesses in grazing animals (Rankama and Sahama, 1949) [25]. The presence of Co and Ni in the above range in the weathering regime at NIASM site indicates that these elements may not cause significant abiotic stress. Copper is biophile and is considered an essential micro-nutrient to plants and its small quantities stimulate plant growth but higher concentrations are known to be toxic in nature (Rankama and Sahama, 1949) [25]. Its presence in the weathering profile in a range of 128-577ppm at the NIASM site is encouraging.

Zinc (Zn) is relatively abundant in basalts and during weathering it readily converts to sulphates and chlorides that dissolve in water. It is an essential element and in low concentrations Zn stimulates healthy growth in plants and animals. However, like Cu, it is toxic in high concentrations. In the samples analysed, Zn concentrations varies from 47 to 107 ppm indicating that the crops cultivated on the NIASM soils would not face zinc deficiency and stresses due to Zn. Molybdenum (Mo) bearing minerals commonly form small quantities of hydrated oxides like molybdnite (MoO_3 or $FeO/3MoO_3.8H_2O$) in the soil profile. However, high Ca in weathering profiles or groundwater could precipitate Mo in calcretes or carbonates. In the samples analysed Mo varies from 1 to 8.5 ppm and it was observed that the subalkaline basalts have higher Mo concentrations as compared to the basaltic andesite samples.

The trace element concentrations of samples from the Main Pit were also plotted as a function of depth (Fig.8). It was observed that there are two prominent trace element anomalies at 50 and 70 cm depth and is similar to the major oxides variation pattern in the Main Pit. The first anomaly is seen at 50 cm depth which is marked by the sudden lowering in the concentrations of trace elements like Zr, V, Cr, Zn, and Co in response to the highly weathered nature of the horizon (red bole). Thereafter is a sharp increase in these trace elements due to the moderately weathered nature of the rock sample analysed that represents the lava toe core. A further lowering of the trace element concentrations is seen at a depth of 70 cm below ground level (BGL) and corresponds to the highly weathered nature of the horizon similar to the upper red bole horizon. It is followed by a gradual increase in the trace element concentrations from 70 cm BGL to 231 cm BGL corresponding to the weathering profile in Lobe 3. This pattern is similar to the major oxide variation in lobe 3 of the Main Pit. The trace element concentration patterns of Cu and Ni appear to have a distinctly opposite signature when compared to trace elements like Zr, V, Cr, Zn, and Co (Fig. 8).

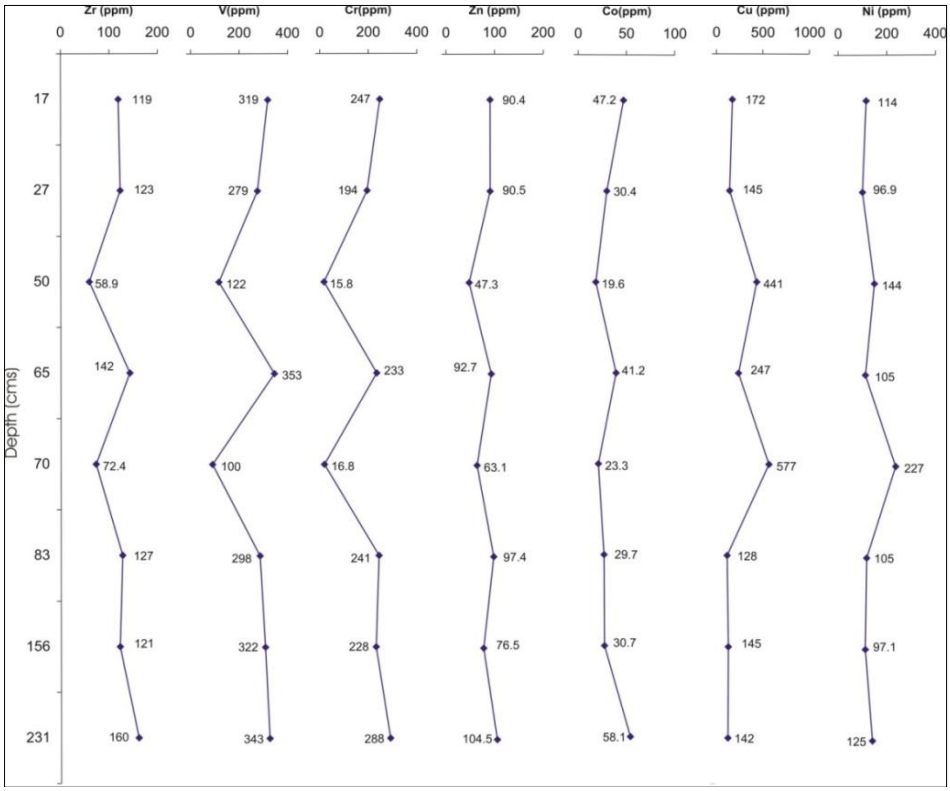

Fig 8: Trace element variation diagram with depth in Main Pit samples from the NIASM site.

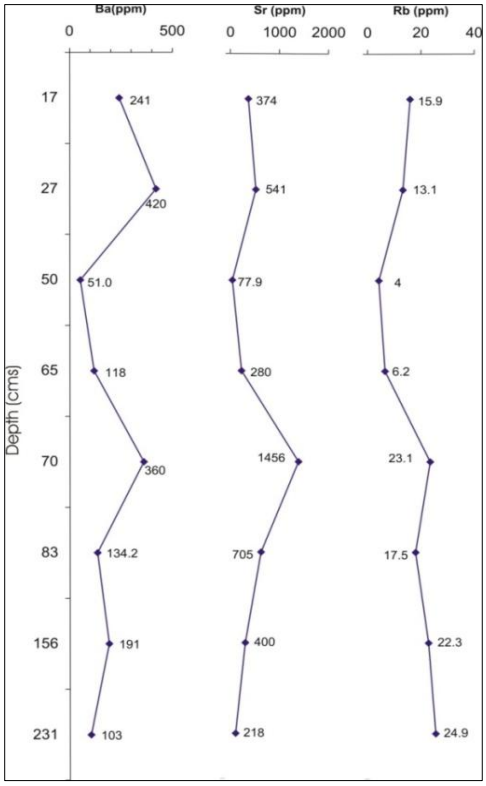

Fig 8 Contd.: Trace element variation diagram with depth in Main Pit samples from the NIASM site.

There are significantly higher concentrations of these elements at depths of 50 cm BGL and 70 cm BGL where the weathering regime in the form of red bole is present. Such anomalous accumulations could suggest that the clays provide suitable suites for their adsorption or that considerable enrichment of these elements takes place due to deposition of soluble salts in an oxidizing environment. There is a wide variation in the trace element patterns of elements such as Ba, Sr and Rb (Fig. 8). They are invariably higher concentration in the upper and lower parts of the Main Pit at NIASM site. This could be the effect either due to the fact that the initial concentrations of these elements may vary in the 3 lava lobes exposed in the Main Pit due to modal variations in the plagioclase content which primarily hosts these trace elements or due to the variable mobility of these elements in response to differential weathering across the Main Pit profile. There is a significant decrease in the concentrations of these element at 50 cm BGL and may be related to the highly weathered nature of the horizon. Since these elements are highly mobile during weathering they leached out from upper horizons under the influence of percolating water during monsoon. The increase of Ba, Sr and Rb at 70 cm BGL could indicate precipitation of these elements at the upper contact of Lobe 3.

5. Conclusions

Study indicated the geochemical variability of major oxide and trace elements are governed by the geological variability in different lava lobe and lava toe geometry of compound pahoehoe as well the degree of weathering. The crystallization of zeolites and other secondary minerals could also influence the trace element distribution in the weathering regime which is apparent due to presence of two anomalies at 50 and 70cm depth.

6. Acknowledgements

Authors are thankful to the Director, National Institute of Abiotic Stress Management, Malegaon, Baramati for providing financial assistance and to the Head, Department of Geology, University of Pune for providing laboratory facilities during the entire course of study. Authors are also thankful to the Er. Pravin More NIASM, Baramati for his technical assistance during the course of prepartion of this manuscriopt.

7. References

1. Aubele JC, Crumpler LS, Elston WE. Vesicle zonation and vertical structure of basalt flows. Jour. Volcanol. Geotherm. Res. 1988; 35:349-374.
2. Beane JE, Turner CA, Hooper PR, Subbarao KV, Walsh JN. Stratigraphy, composition and form of the Deccan basalts, Western Ghats, India. Bull. Volcanol. 1986; 48:61-83.
3. Bondre NR, Duraiswami RA, Dole G. Morphology and emplacement of flows from the Deccan Volcanic Province, India. Bull. Volcanol. 2004; 66:29-45.
4. Duraiswami RA. Pulsed inflation in the hummocky lava flow near Morgaon, Western Deccan Volcanic Province and its significance. Curr. Sci. 2009; 97:313-316.
5. Duraiswami RA, Bondre NR, Managave S. Morphology of rubbly pahoehoe (Simple) flows from the Deccan Volcanic Province: implications for style of emplacement. Jour. Volcanol. Geotherm. Res. 2008a; 177:822-836.
6. Duraiswami RA, Krishnamurthy V, Mitra D, Joshi VB. Modeling salinity in the Karha River Basin: a Remote Sensing and GIS approach. Jr. App. Hydro. 2008b; 20:37-50.
7. Eggleton RE, Foudoulis C, Varkevisser. Weathering of basalt: changes in rock chemistry and mineralogy. Clays and Clay Minerals. 1987; 35:161-169.
8. Geological Survey of India. Quadrangle Geological Map of Baramati Quadrangle. Government of India Press, 1998.
9. Ghodke SS, Powar KB, Kanegoankar NB. Trace elements distribution in Deccan Trap flows in Dive Ghat area, Pune district, Maharashtra. Proc. Symp. Deccan Traps and Bauxites, Geological Survey of India. Spl. Publ. 1984; 14:55-62.
10. Godbole SM, Rana RS, Natu SR. Lava stratigraphy of Deccan basalts of western Maharashtra. Gondwana Geol. Mag. Spl. Publ. 1996; 2:125-134.
11. Kale MG, Dasgupta S. Petrography of Quaternary sediments of Morgaon area, Pune District, Maharashtra, India. Gond. Geol. Mag. 2009; 24:1-10.
12. Kale VS, Patil DN, Pawar NJ, Rajaguru SN. Discovery of volcanic ash bed in the alluvial sediments at Morgaon, Maharashtra. Man and Envi. 1993; 18:141-143.
13. Kale VS, Rajaguru SN. Late Quaternary alluvial history of the northwestern Deccan Upland Region. Nature. 1987; 325:612-614.
14. Kanegaonkar NB, Powar KB. Genesis of Plagioclase megacrysts in porphyritic basalts of Purandhar hills, Western Maharashtra. Recent Res. Geol., Hindustan Publ. Corp, Delhi. 1978; 4:313-332.
15. Khadri SRF, Subbarao KV, Walsh JN. Stratigraphy, form and structure of the east Pune basalts, Western Deccan Basalt Province, India. Geol. Soc. Ind. Mem. 1999; 43:172-202.

16. Korisettar R, Venkatesan TR, Mishra S, Rajaguru SN, Somayajulu BLK, Tandon SK, *et al*. Discovery of tephra bed in the Quaternary alluvial sediments of Pune district (Maharashtra), Peninsular India. Curr. Sci. 1989; 58:564-567.
17. Makki MF. Collecting cavansite in the Wagholi quarry complex, Pune, Maharashtra, India. The Mineralogical Record. 2005; 36:507-512.
18. Maurya UK, Vittal KPR. Geology of the NIAM Site, Malegaon. NIAM Technical Bulletin - 1, National Institute of Abiotic Stress Management (ICAR), Baramati, 2010.
19. Maurya UK, Vittal KPR. Identification of Abiotic Edaphic Stressors of Deccan Trap at NIASM Site, Malegaon: A Geotechnical & Geological Study. NIASM Technical Bulletin-2. National Institute of Abiotic Stress Management (ICAR), Baramati, 2011.
20. Maurya UK, Vittal KPR, Ghadge SV. Formation of zeolites in development of edaphic stressors on Vertic Toposequence. NIASM Technical Bulletin-3. National Institute of Abiotic Stress Management (ICAR), Baramati, 2012.
21. Middlemost. A chemical classification of volcanic rocks based on the total alkali-silica diagram. Jour. Petrol. 1989; 27:745-750.
22. Paranjpe SC. Climatic classification of the Maharashtra State based on methods proposed by Thornwaite. In: An integrated approach for strengthening and protecting drinking water sources, GSDA Seminar Volume, 2001, 489-498.
23. Price J, Velbel MA. Chemical weathering indices applied to weathering profiles developed on heterogeneous felsic metamorphic parent rocks. Chem. Geol. 2003; 202:397-416.
24. Rajguru SN, Kale VS, Badam GL. Quaternary fluvial systems in upland Maharahstra. Curr. Sci. 1993; 64:817-822.
25. Rankama K, Sahama Th. G. Geochemistry. The University of Chicago Press, Chicago, 1949.
26. Verma SP, Torres-Alvarado IS, Sotelo-Rodríguez ZT. SINCLAS: standard Igneous norm and volcanic rock classification system. Computers & Geosciences. 2002; 28:711-715.
27. Wilmoth RA, Walker GPL. P-type and S-type pahoehoe: a study of vesicle distribution patterns in Hawaiian lava flows. Jour. Volcanol Geotherm Res. 1993; 55:129-142.